Lawrence Berkeley National Laboratory

Title
Application of Mathematical Removal of Positron Range Blurring in Positron Emission Tomography

Permalink
https://escholarship.org/uc/item/6b80f1gv

Authors
Haber, S.F.
Derenzo, S.E.
Uber, D.C.

Publication Date
1990-04-01

Lawrence Berkeley Laboratory
UNIVERSITY OF CALIFORNIA

Presented at the IEEE Nuclear Science
Symposium, San Francisco, CA,
January, 15–19, 1990, and to be
published in the Proceedings

Application of Mathematical Removal of Positron Range Blurring in Positron Emission Tomography

S.F. Haber, S.E. Derenzo, and D. Uber

April 1990

Donner Laboratory

Biology & Medicine Division

DISCLAIMER

APPLICATION OF MATHEMATICAL REMOVAL OF POSITRON RANGE BLURRING IN POSITRON EMISSION TOMOGRAPHY

S. F. Haber, S. E. Derenzo and D. Uber
Lawrence Berkeley Laboratory
University of California
Berkeley, CA 94720

April, 1990

APPLICATION OF MATHEMATICAL REMOVAL OF POSITRON RANGE BLURRING IN POSITRON EMISSION TOMOGRAPHY

S. F. Haber, S. E. Derenzo and D. Uber

Lawrence Berkeley Laboratory

University of California, Berkeley, CA 94720

ABSTRACT

The range of positrons in tissue is an important limitation to the ultimate spatial resolution achievable in Positron Emission Tomography. In this work we applied a Fourier deconvolution technique to remove range blurring in images taken by the Donner 600-Crystal Positron Tomograph. Using phantom data, we found significant improvement in the image quality and the FWHM for both ^{68}Ga and ^{82}Rb. These were successfully corrected so that the images and FWHM almost matched those of ^{18}F which has negligible positron range. However, statistical noise was increased by the deconvolution process and it was not practical to recover the full spatial resolution of the tomograph.

1. BACKGROUND

1.1 The Donner 600-Crystal Tomograph

The Donner 600-Crystal Positron Tomograph uses a ring of 600 3-mm-wide BGO scintillator crystals coupled individually to phototubes [1, 2]. High speed parallel electronics detects coincident events and histograms the projection data [3, 4]. Clamshell sampling is used to provide adequate linear sampling [5] in projection bins 0.79 mm wide, corresponding to 12.6 samples/cm and a Nyquist frequency limit of 6.3 cycles/cm. The image is reconstructed by filtering the projections using an AP400 Array Processor and then backprojecting the filtered projections using a IP300 Modular Image Processor. A PDP 11/44 and a VAX 11/780 are used for control and file transfer. This system has 2.6 mm resolution at the center for ^{18}F sources [2].

1.2 Positron Range Blurring

Positrons emitted by a tracer isotope travel a short distance in the tissue and annihilate with an electron to produce two simultaneous, nearly collinear 511 keV photons. This distance is a source of blurring in the reconstructed image.

In earlier work, the positron range distribution was determined by using point sources of positron-emitting isotopes deposited on 6 μm mylar film and surrounded by polyurethane foam [6]. The Donner 280-Crystal Positron Tomograph was used to measure projections through the center of the spherical distribution of positron end points in the foam. An empirical function was fit to the data to determine the projected point spread function q(x) due to range effects alone

$$q(x) = A\, e^{-x/B} + (1-A)\, e^{-x/C}, \qquad (1)$$

where the best fit parameters A, B and C depend on the particular radionuclide (see Table 1). The parameters B and C have been converted to equivalent distances in water.

Table 1. Parameters for the point spread function q(x)

Radionuclide	^{18}F	^{68}Ga	^{82}Rb
Maximum positron energy (MeV)	0.64	1.90	3.35
Best fit parameters of equation 1:			
A	0.851	0.808	0.873
B (mm water)	0.054	0.166	0.222
C (mm water)	0.254	1.15	2.55

Positrons from ^{18}F travel much shorter distances than ^{68}Ga or ^{82}Rb before annihilating. ^{68}Ga or ^{82}Rb images that have been corrected for positron range should look similar to the ^{18}F images.

1.3 Reconstruction Filters

PET images are often reconstructed by Fourier transforming each projection, multiplying by a frequency filter R(f), inverse Fourier transforming the product, and then backprojecting the resulting filtered projections into the image array. The filter with the highest frequency response is the "ramp" filter, whose amplitude

$$R(f) = \frac{|f|}{f_N} \qquad (2)$$

is proportional to the spatial frequency [7]. Equation (2) is normalized to unit amplitude at the maximum recoverable (Nyquist) spatial frequency f_N, which is one-half the sampling frequency (Figure 1).

A frequently used filter is the Shepp-Logan, which is a sine function of the spatial frequency [8] and defined by

$$R(f) = \left(\frac{2}{\pi}\right) \left| \sin\left(\frac{\pi f}{2 f_N}\right) \right|. \qquad (3)$$
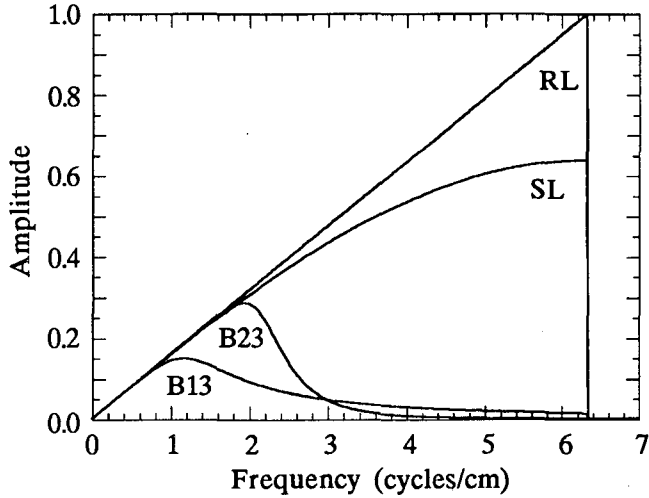
Figure 1. Filters for image reconstruction. RL = "ramp" filter, SL = Shepp-Logan filter, B23 = Butterworth filter with a 90% pass frequency f_p = 2 cycles/cm and a 10% stop frequency f_s = 3 cycles/cm, B13 = Butterworth with f_p, f_s = 1, 3 cycles/cm.

While the sampling used for the 600-Crystal tomograph provides has a Nyquist frequency of 6.3 cycles/cm, there is little image information and significant statistical noise above 4 cycles/cm. Therefore, we commonly reduce the higher frequencies with a generalized Butterworth filter

$$R(f) = \frac{|f / f_N|}{\sqrt{1 + (f / f_c)^{2\eta}}} , \qquad (4)$$

defined in terms of a corner frequency f_c and a coefficient η, which is not necessarily an integer.

It is convenient to describe this filter in terms of a pass frequency f_p and a stop frequency f_s. At the pass frequency the amplitude is 90% of the ramp and $(f_p/f_c)^{2\eta}$ = 19/81. At the stop frequency the amplitude is 10% of the ramp and $(f_s/f_c)^{2\eta}$ = 99. For all the above filters, $R(f)$ = 0 for $|f| > f_N$.

2. CORRECTION FOR POSITRON RANGE

In a previous paper it was shown that Monte Carlo simulations of projection data could be corrected for positron range, and that the statistical noise was increased in the process [9]. In this work, we apply this method to reconstruct projection data of a 37 hot-spot phantom containing ^{18}F, ^{68}Ga, and ^{82}Rb taken with the Donner 600-Crystal Positron Tomograph.

The detected projection data $p(v,\theta)$ are the ideal projection data $d(v,\theta)$ convolved with a function $s(v)$ that describes the positron range

$$p(v,\theta) = s(v) \otimes d(v,\theta) . \qquad (5)$$

The function s(v) is computed by integrating the product of projected point spread function q(v) and the axial response of the tomograph T(z)

$$s(v) = \int_{-g/2}^{+g/2} T(z) q(v') dz , \qquad (6)$$

where g/2 is the tomograph half-gap, $T(z) = 1 - 2 |z|/g$ is the tomograph axial response, and

$$v' = \sqrt{v^2 + z^2} . \qquad (7)$$

The positron end point distribution is spherically symmetric about the source. The function q(v) describes a projection of this distribution through a central plane while the function s(v) includes all of the end points within the tomograph response. The integral in equation (6) was evaluated numerically using adaptive quadrature [10].

Convolution in projection space corresponds to multiplication in frequency space. Therefore the Fourier transform of the measured projection data $P(f,\theta)$ = $\mathcal{F}(p(v,\theta))$ can be represented as the product of the Fourier transforms of the ideal projection data $D(f,\theta)$ = $\mathcal{F}(d(v,\theta))$ and the positron range function $S(f)$ = $\mathcal{F}(s(v))$ [9]

$$P(f,\theta) = S(f) \bullet D(f,\theta) . \qquad (8)$$

To remove the effect of positron range, the Fourier transform of the measured projection data is divided by the Fourier transform of the positron range function

$$D(f,\theta) = P(f,\theta) / S(f) \qquad (9)$$

and the inverse Fourier transform is applied to the quotient

$$d(v,\theta) = \mathcal{F}^{-1}\left(P(f,\theta) / S(f)\right) . \qquad (10)$$

The drawback to this process is that division in frequency space by a function with a low amplitude at high frequencies will boost the high frequencies in the quotient. This will increase the statistical noise while it decreases the systematic error. We will examine this problem quantitatively in the Results Section below.

To include the positron range correction in the normal reconstruction process, we combined the Fourier transform of the positron range function with the Fourier transform of the reconstruction filter R(f) to produce a new filter R'(f) defined by

$$R'(f) = R(f) / S(f) . \qquad (11)$$

In this way the positron range corrections can be incorporated into the usual reconstruction algorithm without increasing the computation time (Figure 2).
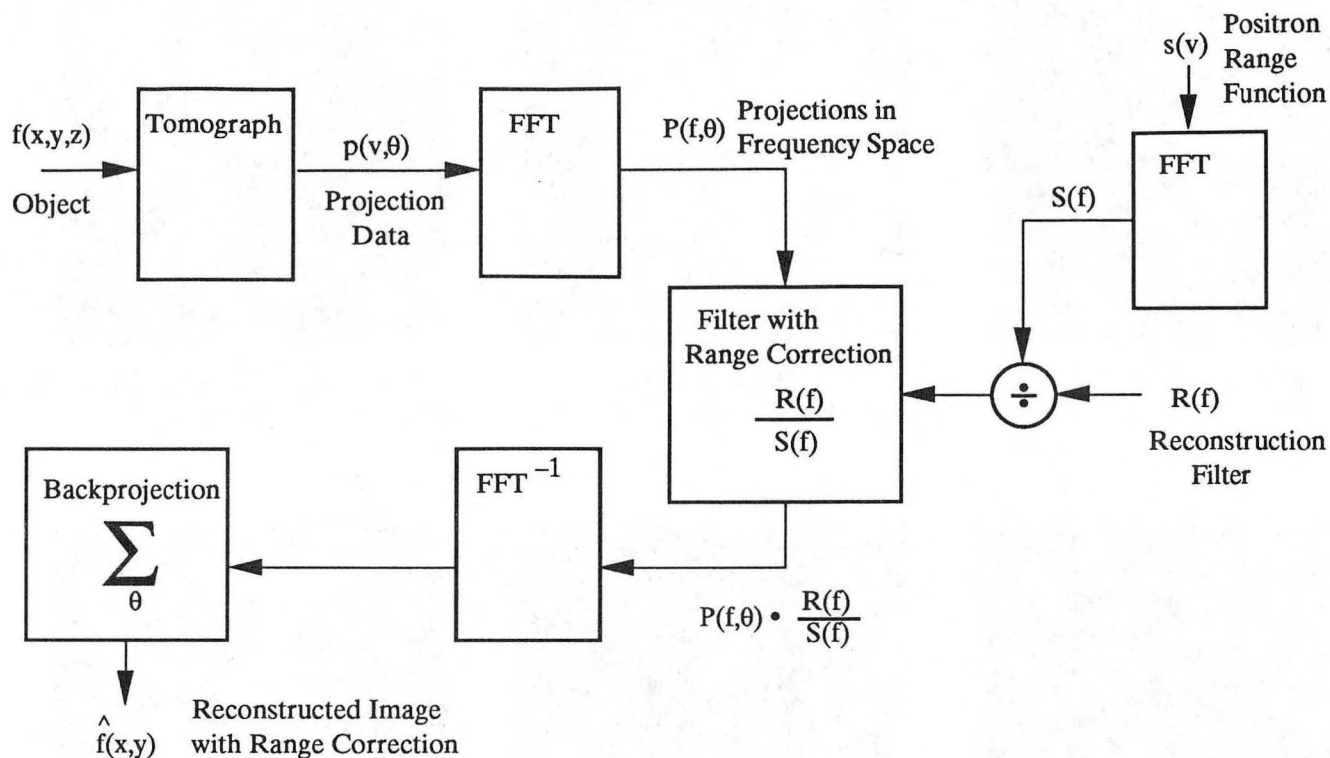
Figure 2. The normal image reconstruction algorithm adapted to include the correction for positron range. The Fourier transform $P(f,\theta)$ of the measured projection data $p(v,\theta)$ is multiplied by the usual filter $R(f)$ and divided by the Fourier transform $S(f)$ of the range blurring function $s(v)$. The result is inverse transformed and backprojected to form the corrected image.

3. RESULTS

3.1 37 Hot Spot Phantom Images

The positron range correction was tested using the 37 point hot spot phantom (Figure 3) with the radionuclides ^{18}F, ^{68}Ga and ^{82}Rb. The resulting PET images are shown in Figure 4 (only the central points of the phantom are included). These demonstrate how well the technique is able to correct the ^{68}Ga and ^{82}Rb data so that the reconstructed images look very similar to that of ^{18}F. The images in the top row show that when using ^{68}Ga and a Butterworth filter with f_p, $f_s = 2$, 3 cycles/cm, the positron range correction can recover an image very similar to ^{18}F. The images in the middle row show that when using ^{68}Ga and a Shepp-Logan filter, the method can correct for ^{68}Ga positron range and provide high resolution images almost of the quality of ^{18}F. The images in the bottom row show that when using ^{82}Rb and a Butterworth filter with f_p, $f_s = 1$, 3 cycles/cm, the positron range correction can improve the imager quality but the resulting image is still inferior to that of ^{18}F.
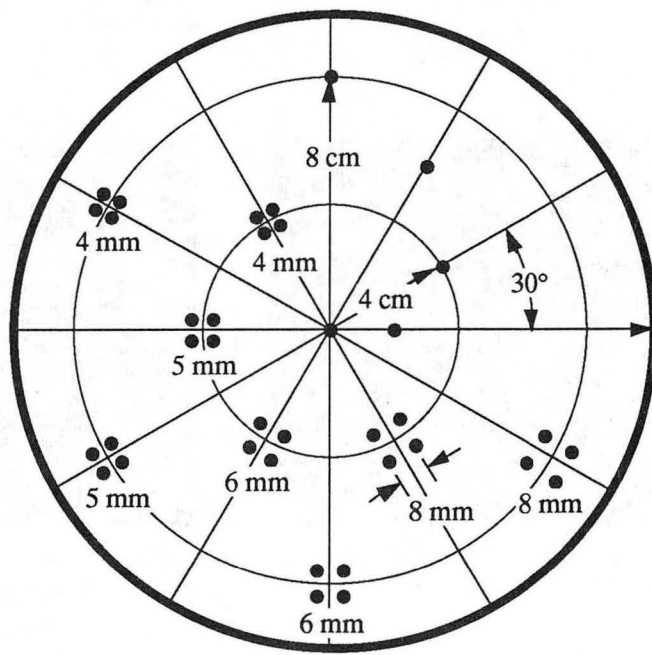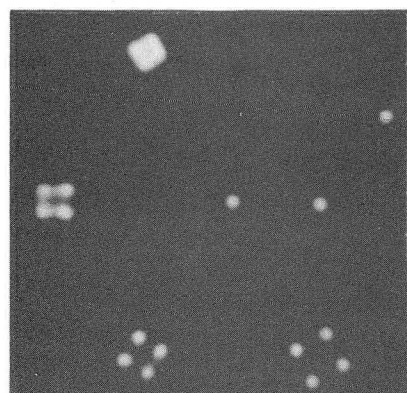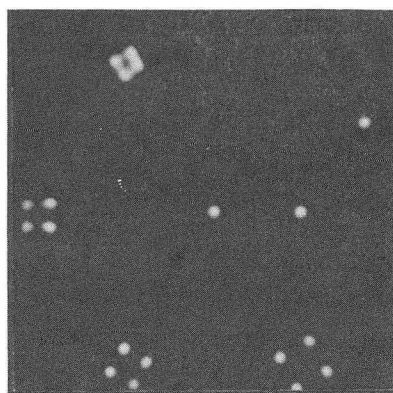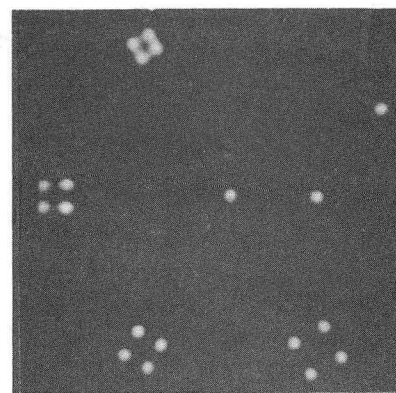

Figure 3. Diagram of phantom with 37 line sources in a 20 cm diameter cylinder of lucite.
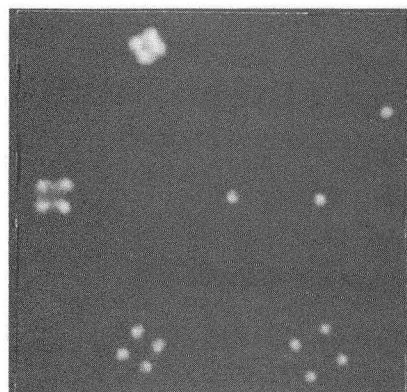
⁶⁸Ga with Butterworth 2, 3 filter
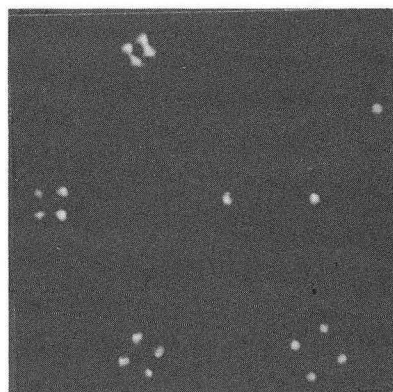
^{68}Ga with Butterworth 2, 3 filter

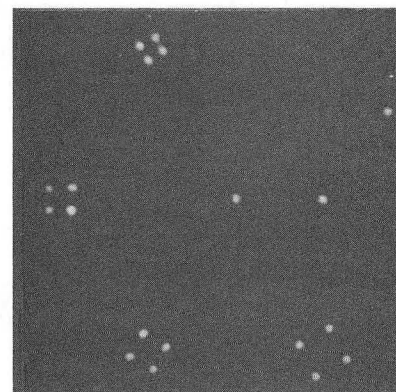^{68}Ga with Butterworth 2, 3 filter and positron range correction

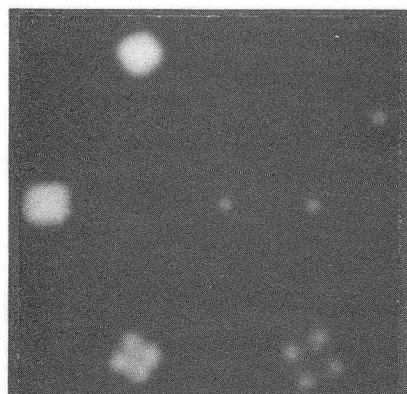^{18}F and Butterworth 2, 3 filter (for comparison)
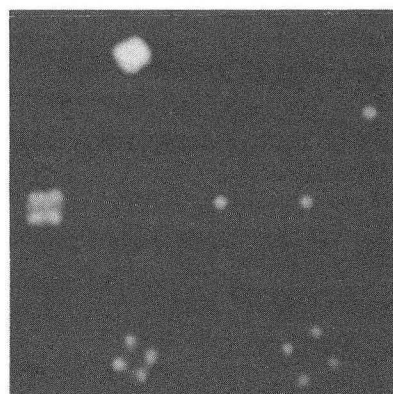
^{68}Ga with Shepp-Logan filter

^{68}Ga with Shepp-Logan filter and positron range correction

^{18}F with Shepp-Logan filter (for comparison)

^{82}Rb with Butterworth 1, 3 filter

^{82}Rb with Butterworth 1, 3 filter and positron range correction
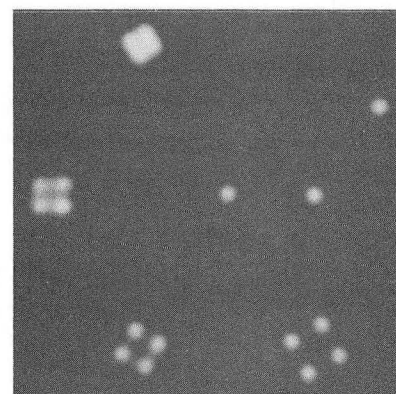
^{18}F with Butterworth 1, 3 filter (for comparison)

Figure 4. The 37-hot-spot phantom imaged with ^{68}Ga and ^{82}Rb isotopes and reconstructed using several reconstruction filters with and without positron range correction. The ^{18}F images have very little positron range blurring and are shown for comparison with the positron range correction.

Plots of the filters used for the reconstructions in Figure 4 can be seen in Figure 5. For both ^{68}Ga and ^{82}Rb, the corrected filters act to boost the high frequencies.

3.2 Profiles of a Single Hot Spot

Intensity profiles along a line through the central hot spot in the reconstructed image of the 37 point phantom were used to determine the widths of the point spread function under various conditions (Table 2).

The range correction is able to reduce the ^{68}Ga full widths at half-maximum and tenth-maximum close to the value for the ^{18}F isotope, whether the Butterworth 2, 3 filter or the Shepp-Logan filter is used. Similarly, the ^{82}Rb full widths at half-maximum and tenth-maximum are close to that of the ^{18}F isotope when the Butterworth 1, 3 filter is used.

The choice of the tomograph gap distance g in equation (6) was varied to see its effect on the FWHM and FW0.1M of the central hot spot in the corrected images. Using g = 0 (and T(z) = 1) in equation (6), the positron range correction is underestimated because end points that do not lie in the central plane are ignored. This causes s(v) to be unrealistically narrow. Using g = ∞ in equation (6), the correction is overestimated because it includes points that do not lie within the axial response of the tomograph. This causes s(v) to be unrealistically broad. By comparison, g/2 = 5 mm gave good agreement between the FWHM and FW0.1M values of the corrected ^{68}Ga and ^{82}Rb data and those of the ^{18}F data.

3.3 Quantitative Evaluation of the Positron Range Correction ; Effect on Statistical Noise.

We used a "flood phantom" to investigate the effect of the positron range correction on the statistical noise in PET images. The flood phantom consisted of a 20 cm diameter plastic cylinder filled with a well mixed solution of water and ^{68}Ga. For low statistics images the intensity variations from one pixel to another are mostly due to statistical noise. For high statistics images some of the variations from one pixel to another are caused by artifacts in the reconstruction process. Note that the number of counts required for a given signal to noise ratio is much higher for the flood phantom than for a typical clinical image that has activity concentrated in a smaller area.

The data for this experiment were recorded in many 60 second data sets that could be added later to vary the total number of events. The images were reconstructed with a pixel size equal to the width of the projection bins (0.79 mm). The mean intensity in the pixels and the rms deviation from that mean (σ) were calculated as a function of the total number of events. The value of the mean divided by sigma should increase linearly with the square-root of the number of events detected.

Plots of mean/σ versus (events)$^{1/2}$ are shown in Figure 6 The flood phantom images were reconstructed using the three filters that we used for ^{82}Rb and ^{68}Ga 37 point phantom images. For each filter, the statistical noise variation is shown for reconstructions with and without positron range correction. The plots show the expected ideal linear relationship when the number of counts is not too high. But, as the number of counts increase, the mean/σ cannot realistically become infinite because it is limited by systematic noise sources.

Table 2. Changes in FWHM and FW0.1M as a Result of Positron Range Correction

| Radionuclide	^{68}Ga	^{68}Ga	^{18}F (for comparison)
Filter Used	Butterworth 2,3	Butterworth 2,3*	Butterworth 2,3
FWHM (mm)	4.12	3.73	3.53
FW0.1M (mm)	7.46	6.09	5.89
Radionuclide	^{68}Ga	^{68}Ga	^{18}F
Filter Used	Shepp-Logan	Shepp-Logan*	Shepp-Logan
FWHM (mm)	3.93	3.34	3.14
FW0.1M (mm)	7.86	5.89	5.30
Radionuclide	^{82}Rb	^{82}Rb	^{18}F
Filter Used	Butterworth 1,3	Butterworth 1,3*	Butterworth 1,3
FWHM (mm)	5.69	4.32	4.16
FW0.1M (mm)	12.96	7.86	7.66

* With positron range correction
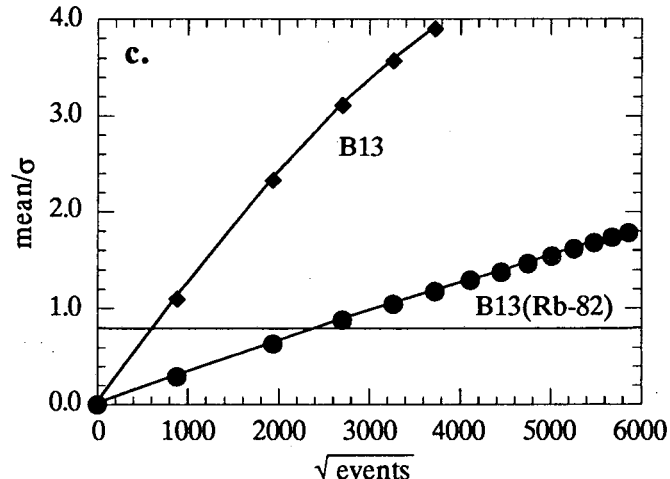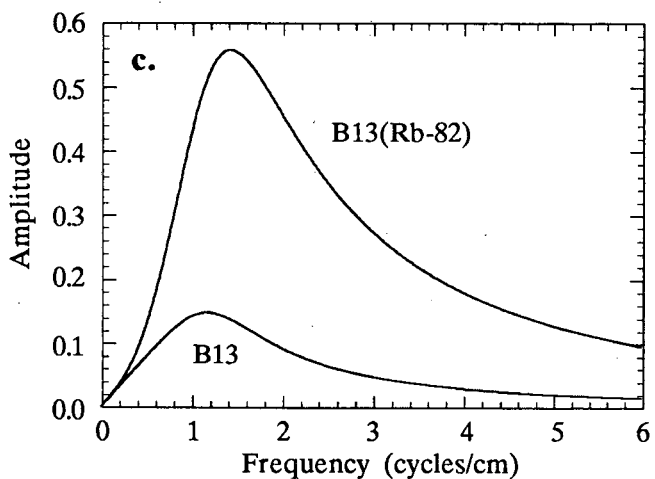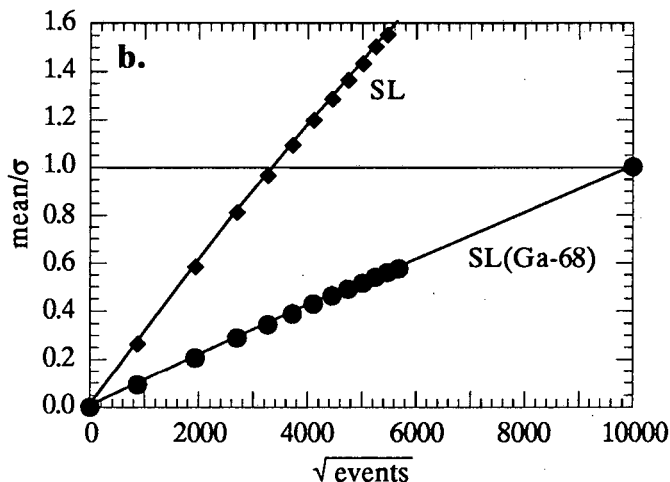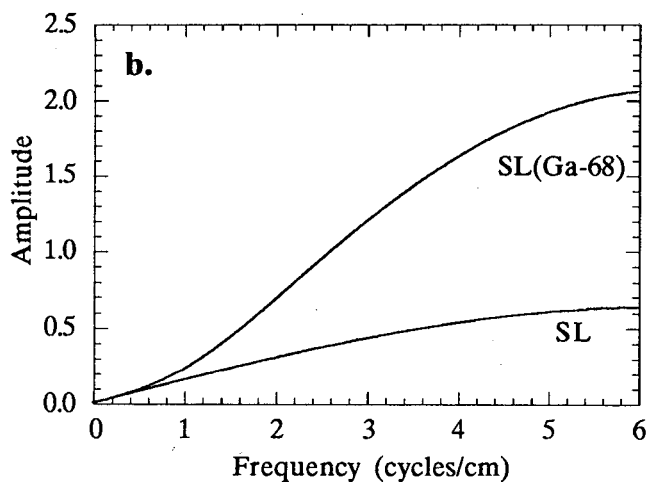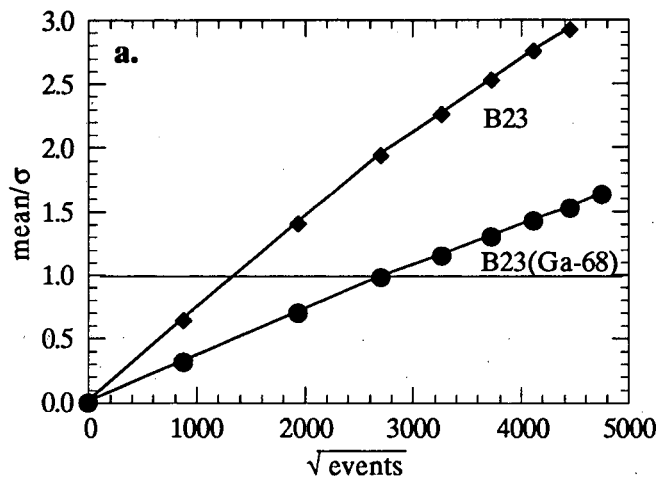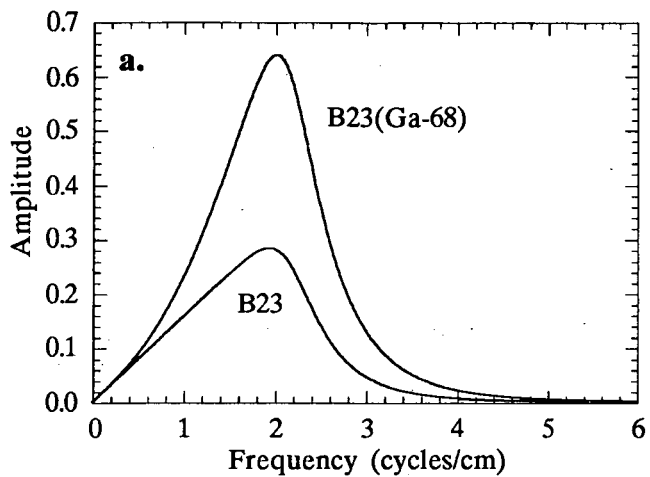
Figure 5. PET reconstruction Filters with and without positron range correction. See below for filter codes.

Figure 6. Signal to noise ratio (mean/σ) as a function of √events. See below for filter codes.

a: B23 = Butterworth 2, 3 filter.   B23(Ga-68) = Butterworth 2, 3 filter with ^{68}Ga range correction.
b: SL = Shepp-Logan filter.   SL(Ga-68) = Shepp-Logan filter with ^{68}Ga range correction.
c: B13 = Butterworth 1, 3 filter.   B13(Rb-82) = Butterworth 1, 3 filter with [82]Rb range correction.

As a means of comparison, the curves were interpolated to find the number of counts that would produce mean/σ = 1 for each case. We can see that for the Butterworth filter with ^{68}Ga positron range correction, the range correction significantly increased the statistical noise. To achieve mean/σ = 1, the corrected data required four times as many counts. When the Shepp-Logan filter was applied, the noise increased even further and the corrected data required nine times as many counts as the uncorrected data for the requirement mean/σ = 1. This increase was expected as the Shepp-Logan filter preserves more of the high frequencies than the Butterworth 2,3 filter does. The noise was highest for the case of Butterworth filter with the [82]Rb range correction, which required sixteen times as many counts to achieve mean/σ = 1. This is plausible, as an extreme correction is needed to reduce the large fraction of annihilations in the tails of the [82]Rb distribution. These results are summarized in Table 3. It does not appear practical to fully recover the full spatial resolution of the tomograph when using [82]Rb.

Table 3. Number of events from 20 cm diameter flood phantom needed to produce mean/σ = 1.

Range Correction	Filter	Before Correction (events)	With Correction (events)	Increase
[68]Ga	B23 *	1.9×10^6	7.6×10^6	×4
[68]Ga	SL †	11×10^6	1.0×10^8	×9
[82]Rb	B13 §	0.6×10^6	9.7×10^6	×16

* B23 = Butterworth filter with f_p = 2 and f_s = 3 cycles/cm.
† SL = Shepp-Logan filter
§ B13 = Butterworth filter with f_p = 1 and f_s = 3 cycles/cm.

4. CONCLUSIONS

We have applied a deconvolution technique to remove the blurring in PET images that is due to positron range. The deconvolution was accomplished by taking the Fourier transform of a function that models the positron range function (for a given radionuclide) and dividing it into the transform of the data. This frequency space approach was particularly convenient because the positron range correction could be easily combined with the normal reconstruction process.

Applying the corrected filters to actual phantom data, we found significant improvement in the quality of the images and the FWHM for both ^{68}Ga and [82]Rb. These were successfully corrected so that the images and the FWHM almost matched those of ^{18}F which has negligible positron range in the context of current PET resolution limits.

However, the division in frequency space leads to increased statistical noise. This noise amplification effect can be reduced by limiting the high frequency response of the reconstruction filter, such as with the generalized Butterworth filter. Thus, it is necessary to choose a balance between the restoration of high spatial frequencies and the noise in the reconstructed image.

REFERENCES

[1] S. E. Derenzo, R. H. Huesman, J. L. Cahoon, et al., "Initial results from the Donner 600 crystal positron tomograph," *IEEE Trans Nucl Sci*, vol. NS-34, pp. 321-325, 1987.

[2] S. E. Derenzo, R. H. Huesman, J. L. Cahoon, et al., "A positron tomograph with 600 BGO crystals and 2.6 mm resolution," *IEEE Trans Nucl Sci*, vol. NS-35, pp. 659-664, 1988.

[3] J. L. Cahoon, R. H. Huesman, S. E. Derenzo, et al., "The electronics for the Donner, high resolution 600-crystal positron tomograph," *IEEE Trans Nucl Sci*, vol. NS-33, pp. 570-574, 1986.

[4] B. T. Turko, G. Zizka, C. C. Lo, et al., "Scintillation photon detection and event selection in high resolution positron emission tomography," *IEEE Trans Nucl Sci*, vol. NS-34, pp. 326-331, 1987.

[5] R. H. Huesman, S. E. Derenzo and T. F. Budinger, "A two-position sampling scheme for positron emission tomography" *Nuclear Medicine and Biology, Vol I,* 542-545, 1983.

[6] S. E. Derenzo, "Precision measurement of annihilation point spread distributions for medically important positron emitters" In *Positron Annihilation,* 819-823, (Edited by R. R. Hasiguti and K. Fujiwara), The Japan Institute of Metals, Sendai, Japan, 1979.

[7] G. N. Ramachandran and A. V. Lakshminarayanan, "Three-dimensional reconstruction from radiographs and electron micrographs: application of convolutions instead of Fourier Transforms," *Proc Nat Acad Sci US,* vol. 68, pp. 2236-2240, 1971.

[8] L. A. Shepp and B. F. Logan, "The Fourier Reconstruction of a head section," *IEEE Trans Nucl Sci,* vol. NS-21(3), pp. 21-43, 1974.

[9] S. E. Derenzo, "Mathematical removal of positron range blurring in high resolution tomography," *IEEE Trans Nucl Sci,* vol. NS-33, pp. 565-569, 1986.

[10] S. E. Derenzo, "INTERFACING: A Laboratory Approach Using the Microcomputer for Instrumentation, Data Analysis and Control", Prentice-Hall, Englewood Cliffs, NJ, pp 329-333, 1990.